Applied Energy 323 (2022) 119563

Contents lists available at ScienceDirect

Applied Energy

journal homepage: www.elsevier.com/locate/apenergy

Creating a Solar-Powered Drip Irrigation Optimal Performance model (SDrOP) to lower the cost of drip irrigation systems for smallholder farmers

Fiona Grant [a,b,*,1], Carolyn Sheline [a,b,1], Julia Sokol [a,b], Susan Amrose [a,b], Elizabeth Brownell [a,b], Vinay Nangia [c], Amos G. Winter V [a,b]

[a] Massachusetts Institute of Technology (MIT), USA
[b] MIT Global Engineering and Research (GEAR) Lab, USA
[c] International Center for Agricultural Research in the Dry Areas (ICARDA), Rabat, Morocco

ARTICLE INFO

Keywords:
Solar power
Drip irrigation
Energy management
Smallholder agriculture
Particle swarm optimization

ABSTRACT

Smallholder farmers, who hold 84% of the approximately 570 million farms worldwide, are vital stakeholders in the process of sustainable agricultural intensification, but often lack the capital to invest in sustainable farming practices. Solar-powered drip irrigation has the potential to increase crop productivity for minimal water use, but these systems are prohibitively expensive for smallholders. Reducing the life cycle cost (LCC) of solar-powered drip irrigation systems could make this technology more accessible, enabling smallholders to increase their household incomes and contribute to greater global food security. This paper presents the Solar-Powered Drip Irrigation Optimal Performance model (SDrOP), which optimizes solar-powered drip irrigation system designs. Unlike existing commercial software, SDrOP models the behavior of the entire system and simulates seasonal performance to reduce LCC while maintaining operational reliability. SDrOP improves on previous design optimization frameworks by taking in all location-dependent parameters as inputs, which makes the model independent of case specifics and, therefore, broadly applicable. To demonstrate the model theory, the sensitivity of the optimal design to field area, the system reliability constraint, and varying weather conditions are explored for a Moroccan olive orchard case study. The results demonstrate opportunities for system cost reduction, including operational changes to reduce the system power requirement, irrigation pump opportunities for the smallholder market, and reductions in system reliability when it is shown to have minimal impact on crop yield. When benchmarked against a commercially available software, SDrOP was able to reduce system LCC by up to 56%. The simulated performance of an SDrOP optimal design was benchmarked against operational data from an existing field site, and was shown to be capable of operating 92% of the recorded irrigation events. These results indicate that SDrOP offers an advantage over existing software as it produces significantly reduced cost designs that can operate in real-world conditions.

1. Introduction

Food security is a growing global issue accelerated by the effects of rapid population growth and climate change. The increasing demand for food puts additional strain on agricultural practices; sustainable agricultural intensification, or increasing the productivity of existing cropland, is necessary to meet the growing demand [1]. A vital stakeholder to engage in this process is smallholder farmers, who typically work plots of land that are two hectares or less and hold 84% of the approximately 570 million farms worldwide [2]. Smallholders have a vast knowledge of local conditions and methods to maintain biodiversity, but are often forced to use unsustainable practices due to a lack of access to capital, information, or agricultural inputs [1]. As a result, smallholders tend to be cost-sensitive and risk-averse [1,3]. Studies have shown that smallholdings can be more productive per hectare than large farms [4,5], and when they are able to increase their income, smallholders have been shown to stimulate rural economies by spending locally and creating labor jobs [5]. Increasing sustainable, efficient irrigation methods among smallholders can enable them to increase crop productivity and household incomes [6,7].

Drip irrigation is a micro-irrigation technology that releases a controlled volume of water and nutrients to the root zone of the crop through a network of pipes and drip emitters. It has been shown

* Corresponding author at: Massachusetts Institute of Technology (MIT), USA.
E-mail addresses: fionag@mit.edu (F. Grant), csheline@mit.edu (C. Sheline), sokol@mit.edu (J. Sokol), samrose@mit.edu (S. Amrose), ebrownll@mit.edu (E. Brownell), v.nangia@cgiar.org (V. Nangia), awinter@mit.edu (A.G. Winter V).
[1] Co-lead authors, contributed equally to this work.

https://doi.org/10.1016/j.apenergy.2022.119563
Received 27 January 2022; Received in revised form 2 June 2022; Accepted 26 June 2022

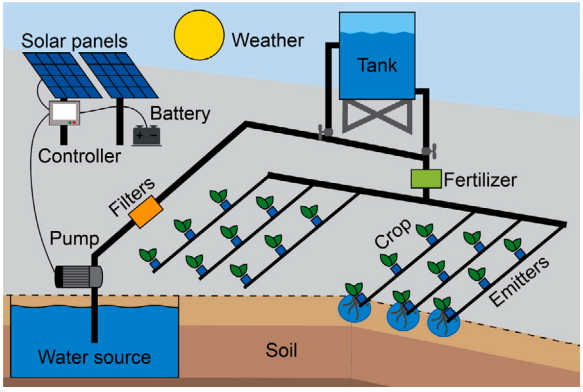

Fig. 1. A solar-powered drip irrigation system consists of a power system, a pump, a hydraulic pipe network, and emitters. The subsystems are highly interdependent during system operation.

that replacing inefficient irrigation methods with drip irrigation could reduce water wasted during irrigation by 20 to 76% and increase crop water productivity by 15% [8]. By adopting drip irrigation, smallholders could increase crop productivity while conserving water. Despite these benefits, drip irrigation is not widely adopted among smallholders because of its high capital cost and increased labor requirements compared to traditional irrigation methods, such as flood and furrow irrigation [1,9,10]. In addition, the majority of smallholders live in rural areas and have limited access to fuel and electricity [3]. This means they require off-grid power sources, which have high upfront costs. The aim of this work is to create an optimization design tool that minimizes the cost of solar-powered drip irrigation systems for smallholder farmers.

A solar-powered drip system (Fig. 1) is comprised of subsystems that have a cyclic interdependence as the system operates. The local weather patterns, soil properties, and the selected crop determine the crop water demand; the water demand and hydraulic network layout determine the required pumping power; and the power available to operate the pump is determined by the power system capacity and the local weather patterns. Existing commercial tools for designing drip irrigation systems model these subsystems independently, without accounting for their dynamic interactions, and have component limitations. EPANet [11], IrriCAD [12], and IrriPro [13] can simulate the pipe network hydraulic behavior, but cannot simulate crop water demand, select a pump, or size an off-grid power system. Industrial pump companies, such as Lorentz, Grundfos, and Xylem, have web applications that facilitate pump selection, but these tools are limited to the pump catalogs of each company [14–16]. Lorentz also offers Compass [14], a desktop tool specifically for sizing solar-powered pumping systems. While Compass does take in some location-specific parameters, it does not account for the relationship between variation in crop water demand and variation in available solar power when sizing the solar panel array. Each of these software tools can accurately capture the behavior of a single subsystem, but they lack a coherent way to leverage the subsystem relationships to reduce the overall drip system cost. A holistic tool would model the behavior of all subsystems and capture subsystem interactions by simulating system operation over an irrigation season for any location and crop type. Previous work conducted by the authors has shown that this holistic, generalizable design approach can lead to a significant reduction in drip system capital cost compared to designs produced by commercial software tools [17,18].

There is a growing body of work on holistic modeling and optimization of drip irrigation and solar-powered pumping systems. Multiple studies explore the feasibility of these technologies in the context of smallholder farming, which provides valuable insights on the constraints and needs of smallholders, but these studies do not attempt to reduce cost or optimize the system design [19,20]. Further work has been conducted to optimize the system design by modeling the behavior and interactions of multiple subsystems. Bakelli, et al. [21] presents a cost-optimization method for sizing a solar-powered pumping system, accounting for the dynamics of solar power availability and water storage in an elevated tank. Muhsen, et al. [22] presents a multi-objective optimization scheme for sizing solar-powered pumping systems. These papers include system life cycle cost models and useful measures of performance reliability that depend on system operation; both concepts are essential to a holistic design tool. The one drawback is that these optimization approaches are difficult to generalize outside of the cases presented in the studies. Bakelli, et al. [21] uses a polynomial fit to experimental hydraulic data, rather than an analytical fluid mechanics model, which makes it difficult to apply to other hydraulic network configurations. Muhsen, et al. [22] uses parametric component models that are more broadly applicable. However, the weights used on each objective function in their multi-objective optimization are determined by a survey of three experts whose area of expertise is not provided, making it difficult to generalize this approach. The conditions smallholders face are varied and highly location-dependent. In designing systems for smallholders, who are both cost-sensitive and risk-averse, there is a need for a holistic design framework that is agnostic to case-specific details and, therefore, easily generalizable to a variety of cases.

This paper presents the Solar-Powered Drip Irrigation Optimal Performance model (SDrOP), a holistic model that accurately captures subsystem relationships and employs a particle swarm optimization (PSO) algorithm to produce optimal low-cost, solar-powered drip system designs. SDrOP takes in all location-dependent parameters as inputs, making it broadly applicable to a variety of contexts. In this paper, SDrOP is used to determine the sensitivity of the system architecture to these location-dependent inputs, and the model is benchmarked against a commercial software. The analytical results demonstrate opportunities for system cost reduction, which could improve the accessibility of drip irrigation to smallholder farmers. These include changes to the system operation to reduce operating power and power system capacity, market opportunities for irrigation pumps that specifically meet the needs of smallholders, and slight reductions in system reliability in cases where it is shown to have a minimal impact on crop yield. Previous work has been done by our research group to develop a novel pressure compensating (PC) emitter that can reduce the required pumping power by 30%–60% compared to commercial emitters, while maintaining comparable flow performance [23,24]. The reduction in pumping power can enable drip system designs with smaller, less expensive pumps and power systems. These emitters are used for the analyses presented in this paper to examine how their novel performance characteristics can be leveraged to reduce overall system cost.

Morocco was selected as a representative candidate country for studying the adoption of solar-powered drip irrigation by smallholders and demonstrating the SDrOP model capabilities. As a country in the Middle East and North Africa (MENA) region, it has an arid climate and high solar irradiance, and the Moroccan government is actively engaged in promoting the adoption of drip irrigation technology among smallholders through subsidies [10]. A representative field of olive trees in Marrakesh, Morocco is employed as a case study to demonstrate the model theory through simulations and a small-scale field experiment. The operational data from this experiment are used to validate the predicted performance of an optimal system design produced by SDrOP. These analytical and experimental results give confidence that SDrOP can produce feasible designs for real-world conditions and provide insights on system cost trade-offs to component selection, system operation, reliability, and weather variability, some of which are case-specific and others that can be applied more broadly. SDrOP may be a useful tool for companies and contractors who design drip systems, and the analytical framework presented in this paper may be of interest to researchers designing stand-alone, solar-powered pumping systems.

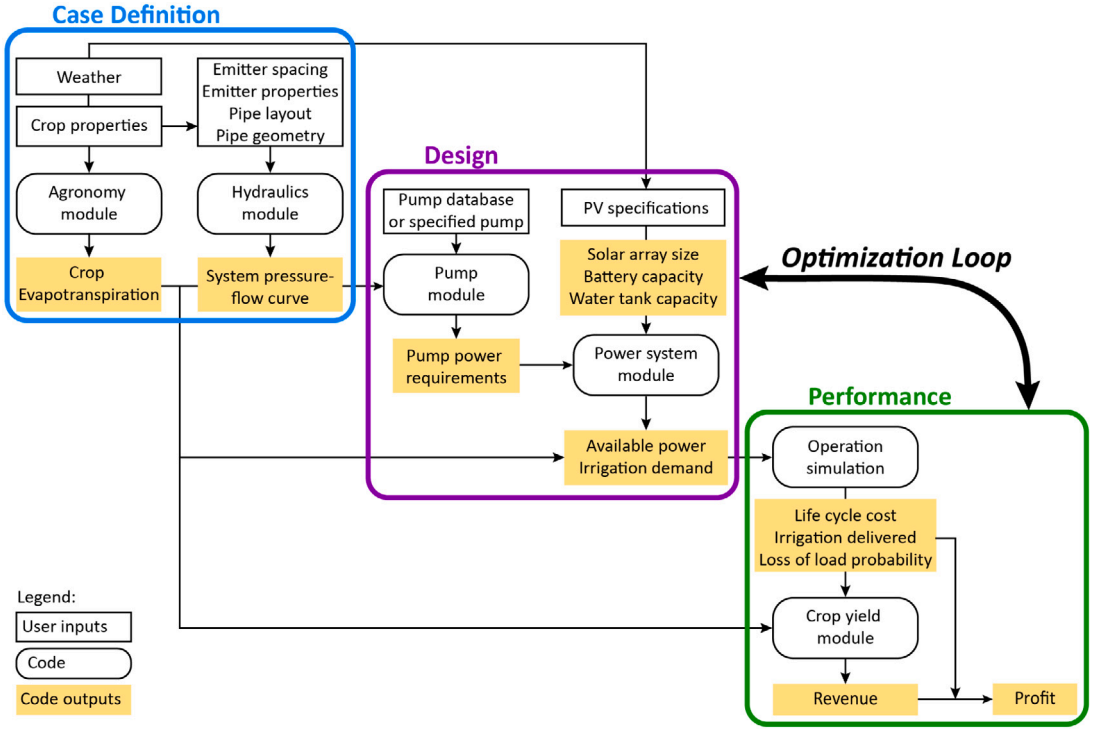

Fig. 2. The SDrOP model architecture and its three computational phases: Case Definition, Design, and Performance. The modules in the first two phases represent the four subsystems of a drip irrigation system, and the last phase assesses the performance of the proposed system design by simulating the system operation. The optimization loop iterates between the Design and Performance phases to select an optimal low-cost design. The user inputs (outlined black boxes), are location-specific and include the cost data for each component. The code outputs (shaded boxes) show how the crop water demand (evapotranspiration) and the hydraulic network operating curve are translated into a system operating point, which is then used to select a pump and design a power system. The design is analyzed by simulating its operation and crop yield over a growing season and computing its life cycle cost (LCC) and lifetime profit.

2. Analytical theory and implementation

2.1. SDrOp model architecture

SDrOP is structured as a set of six modules, implemented in MATLAB, that capture the behavior of the drip irrigation subsystems. The agronomy module captures the relationship between the crops and local environmental conditions; the hydraulics module simulates the behavior of the hydraulic network; the pump module links the hydraulic load to the required pumping power; the power system module relates the power requirement to the local weather patterns; the operation module synthesizes these subsystem relationships in a simulation of the system operation over a growing season; and the yield module estimates the crop yield based on the system performance. The optimization loop iterates through permutations of pump and power system designs to converge on an optimal combination. The objective of the optimization can be set to either minimize the system life cycle cost (LCC) or maximize its lifetime profit. This architecture enables SDrOP to capture the behavior of a solar-powered drip system and leverage the subsystem relationships when optimizing the system design.

Smallholder farming use cases can vary widely depending on the crops selected, field layout, farming practices, and local environmental conditions. SDrOP is structured to accommodate this variability, making it a broadly applicable design tool. This is accomplished by decoupling location-specific information for a given case from the physics-based theory that describes the drip system behavior. The modules described above fall into three distinct computational phases: Case Definition, Design, and Performance (Fig. 2). In each phase, the inputs are location-specific, but the theory describing the behavior of each subsystem is parametric and, therefore, generalizable.

The inputs to the Case Definition phase include local weather data, local soil and crop properties, crop spacing on the field, the depth of the water source, equipment specifications for locally-available components, and estimates of the local prices of the components and crop produce. The parameters needed to determine the crop water demand are computed using an agronomic model, and the drip system operating point is computed with an iterative fluid network calculation. This information is passed into the Design phase, where a pump is selected and a power system is sized using equipment specifications for locally-available components. Finally, in the Performance phase, the operation of the proposed drip system design is simulated over the course of a full growing season for the selected crop. This phase also computes the system LCC, the lifetime profit based on estimated crop yield, and the system reliability in delivering water to the crop. The details of each module and the optimization are presented in the following sections.

2.2. Subsystem module definitions

The following sections present the fundamental theory behind each of the six SDrOP modules. The specific parameters that define a case are given in Section 2.4.

2.2.1. Agronomy module

The crop evapotranspiration, or the amount of water that is released from the soil and the crop leaves, is used to compute the crop water demand for the drip system. The evapotranspiration calculation within the agronomy module is validated in the FAO Irrigation and Drainage Paper No. 56 [25].

The crop evapotranspiration (ET_c [mm/day]) is calculated as

$$ET_c = K_c\, ET_0, \tag{1}$$

where K_c is a crop coefficient and ET_0 is the reference evapotranspiration [mm/day]. ET_0 is calculated for a grass reference crop of 0.12 m

height using the standard method of the Penman–Monteith equation:

$$ET_0 = \frac{0.408\delta(G_{net} - HF_s) + \gamma \frac{900}{T+273} u_2 (e_s - e_a)}{\delta + \gamma(1 + 0.34u_2)}, \quad (2)$$

where G_{net} is the net irradiance at the crop surface [MJ/m^{2}day], HF_s is the soil heat flux density [MJ/m^{2}day], T is the daily or hourly average air temperature at 2 m height [°C], u_2 is the wind speed at 2 m height [m/s], e_s is the saturation vapor pressure [kPa] at air temperature T, e_a is the actual vapor pressure [kPa], δ is the slope of vapor pressure curve [kPa/°C] at air temperature T, and $\gamma = 0.665 \times 10^{-3} p_{atm}$ is the psychrometric constant [kPa/°C]. The atmospheric pressure [kPa], p_{atm}, is determined from altitude using a simplification of the ideal gas law and assuming an atmosphere at 20 °C. Temperature, relative humidity, solar irradiance, and wind speed are generally available for weather stations in publicly accessible databases, such as ASHRAE weather files [26]. For this work, the weather data used are IWEC2 [27], and they were selected from a station that was closest to the location of interest.

Eq. (1) assumes a single crop coefficient, K_c, which is a function of the crop and its development stage. The length of the development stages and K_c values corresponding to each stage of development – $K_{c,ini}$, $K_{c,mid}$, $K_{c,end}$, for the beginning, middle, and end stages, respectively – are defined in [25]. The single K_c assumes a well watered standard crop that is subjected to typical growing conditions and a sub-humid climate with a mean minimum relative humidity ($RH_{min,mean}$) of 45% and a mean wind speed at 2 m ($u_{2,mean}$) of 2 m/s. For $RH_{min,mean}$ and $u_{2,mean}$ values outside of the sub-humid conditions, the coefficients are adjusted given

$$K_{c,mid/end,adj} = K_{c,mid/end} + (0.04(u_{2,mean} - 2) - 0.004(RH_{min,mean} - 45))\left(\frac{h}{3}\right)^{0.3}, \quad (3)$$

where $K_{c,mid/end}$ is the sub-humid standard value for $K_{c,mid}$ or $K_{c,end}$, h is the mean plant height during the mid/late-season stage [m], and values of $u_{2,mean}$ and $RH_{min,mean}$ are calculated from weather inputs for the corresponding growth stage. Note that field-specific calibration of the K_c is needed for accurate crop evapotranspiration calculations.

The agronomy module calculates daily ET_c and its variation with weather conditions (details are provided in the SI Section 1). Capturing these variations allows for the design of a more exact system size compared to using a single average value for crop evapotranspiration and water demand [17].

2.2.2. Hydraulics module

The hydraulics module computes the system operating point based on the specifications of the hydraulic network in the case definition. The hydraulic network consists of a main pipe that originates at the pump, submain pipes that branch off of the main, and laterals that connect to the submain and run the length of the crop row. It is assumed that the emitters are equally spaced along each lateral at the crop spacing given in the case definition [17]. For all cases presented herein, the hydraulic network is modeled with pressure compensating (PC) emitters. The system operating point is the pressure head and flow rate required to operate the hydraulic network. The module iteratively converges on the system flow rate for a range of input pressures, which results in the steady state system operating curve shown in Fig. 3. Major pressure losses in the pipe network are calculated using the Darcy–Weisbach equation:

$$\Delta p_{major} = f_d \frac{L}{D} \frac{\rho v^2}{2}, \quad (4)$$

where f_d is the Darcy friction factor, L and D are the pipe length [m] and inner diameter [m], ρ is the density of water [kg/m^2], and v is the flow velocity [m/s]. Minor pressure losses are estimated using

$$\Delta p_{minor} = K_{minor} \frac{\rho v^2}{2}, \quad (5)$$

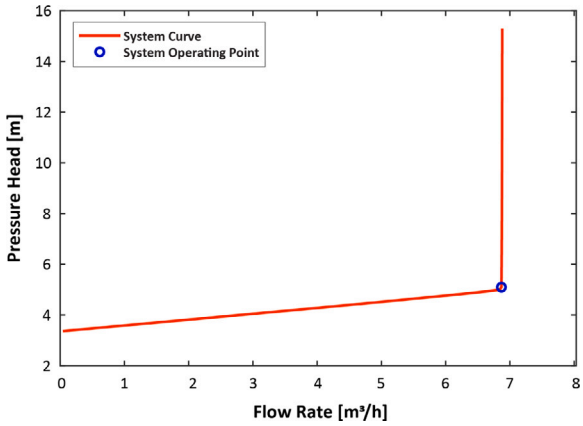

Fig. 3. The hydraulic system curve of a drip system using pressure compensating (PC) emitters. The curve shows the pressure compensating behavior introduced by the emitters. The flow rate increases with pressure until the last emitter has reached its activation pressure, at which point the flow rate remains constant. The ideal, minimum power operating point for the system is just after this slope change (circle).

where K_{minor} is the minor loss coefficient. Minor losses are modeled for tee fittings at the start of each submain and lateral, where $K_{minor} = 1$ for tee losses in branch flow [28]. Minor losses due to additional fittings, such as valves and elbows, are estimated to be constant at 0.01 bar. This estimate for minor losses is based on previous field trail data used to validate the hydraulics module [18]. The Darcy friction factor, f_d, is computed using the Swamee–Jain formula [29]:

$$f_d = \frac{0.25}{[log_{10}(\frac{\epsilon}{3.7D} + \frac{5.74}{Re_D^{0.9}})]^2}, \quad (6)$$

where Re_D is the Reynolds number and ϵ is the pipe roughness [m]. The pressure losses across the sand and disk filters are calculated using

$$\Delta p_f = a e^{bQ_{sys}}, \quad (7)$$

which is an empirical estimation from the manufacturer [30]. Here, Δp_f is pressure loss across the filter [bar], Q_{sys} is the system flow rate [m^3/h], and a and b are constants that can be found in filter specification sheets. The fertigation unit is assumed to be a mixing tank connected in parallel with the main pipe, which is based on low-pressure, commercially available units [31].

The flow rate of the PC drip emitters is approximately constant for emitter pressures, p_{em}, above their activation pressure, p_{act} [bar]. The emitter flow rate is therefore modeled as linear when $0 < p_{em} < p_{act}$, and as $Q_{em} = k_{em} p_{em}^{x_{em}}$ when $p_{em} \geq p_{act}$, where k_{em} is the flow coefficient and x_{em} is the pressure compensation exponent. Pressure losses due to water flowing over the protrusion of the emitter into the lateral, which are small compared to the pressure drop inside the emitter, are neglected.

Due to the pressure compensating behavior of the emitters, the system curve has a unique shape (Fig. 3). As the system pressure increases, the system flow rate increases until all of the emitters in the network are at or above their activation pressure and emitting water at their nominally constant flow rate. The inflection point between these two regimes is the ideal, minimum power operating point for the system, henceforth called the system operating point. Increasing pressure beyond this point will result in over-pressurizing the pipes without producing a higher flow rate. Because hydraulic power is the product of the system pressure head and flow rate, $P_{hyd} = H_{sys} \times Q_{sys}$, operating above this point wastes power. The hydraulics module identifies the inflection point on the system curve and passes the system operating point into the pump module.

2.2.3. Pump module

The pump module determines the required pumping power for the system operating point calculated in the hydraulics module by selecting pumps from a database of locally-available pump architectures. Integrating the pump database with SDrOP allows for a wide range of pump architectures to be searched for any given case, which facilitates the selection of feasible pumps. For a pump to be feasible, the system flow rate must be within the pump POR, which is the region of pump flow rates that are within 70 to 120% of the best efficiency point (BEP) flow rate. This operating region is recommended by pump manufacturers to ensure the pump lasts its rated lifetime [32]. Requiring that the system operating point fall within the POR of any selected pumps also ensures that the pumps operate near their BEPs, which in turn enables the design of smaller, less expensive power systems.

The pump database contains the characteristic curves of each pump, which are the performance (pressure head-flow rate) curve, the efficiency-flow rate curve, and the power-flow rate curve. In general, a pump will operate at the pressure head and flow rate where the system curve and pump performance curve intersect. However, it is not guaranteed that the system curve will intersect the pump performance curve exactly at the system operating point. To ensure that the selected pumps operate the hydraulic network at the desired point, it is assumed that each pump is paired with a motor driver that can change the motor speed. Changing the pump motor speed shifts the pump characteristic curves, which expands the operating range of the pump. This enables the pump module to determine the pumping power of the pump operating point that exactly matches the system operating point.

For each feasible pump, the motor speed is selected such that the corresponding pump performance curve intersects the system curve at the system operating point (Fig. 4). The affinity laws for centrifugal pumps describe how the characteristic curves shift with varying motor speed:

$$\frac{Q_{new}}{Q_{ref}} = \frac{N_{new}}{N_{ref}}, \tag{8}$$

$$\frac{H_{new}}{H_{ref}} = \left(\frac{N_{new}}{N_{ref}}\right)^2 \tag{9}$$

and

$$\frac{P_{new}}{P_{ref}} = \left(\frac{N_{new}}{N_{ref}}\right)^3, \tag{10}$$

where Q is flow rate, H is pressure head, P is power, and N is rotational speed. Here, the ref values correspond to the curves at the reference motor speed and the new values correspond to the curves at the new motor speed. These laws are established scaling relationships that use the known characteristic curves at one speed to predict the characteristic curves at another speed for a given impeller diameter [33].

Fig. 4 provides a visualization of how the affinity laws are used to identify the required pumping power. The reference pressure head, H_{ref}, is the pressure head corresponding to Q_{sys} on the pump performance curve from the database. The corresponding motor speed, the desired system operating pressure head identified in the hydraulics module, and H_{ref} are used in Eq. (9) to compute the desired pump speed, N_{new}. This is the speed of the pump characteristic curve that will exactly intersect the system operating point. Once the desired pump speed is known, the pump characteristic curves from the database can be used as the reference to compute the characteristic curves at the desired pump speed using the affinity laws (Eqs. (8)–(10)). The new power-flow curve is then used to identify the required pumping power for the system. A similar process is employed to compute the pump operating point when pumping water to a tank for a system design that includes water storage (details of the pump-to-tank simulation are included in the SI Section 3).

The SDrOP pump database consists of centrifugal, surface pumps with AC motors. Centrifugal pumps are ubiquitous [34] and, based on conversations with local contractors, the performance characteristics of the selected pumps were representative of locally-available pumps in Morocco [10] (see Appendix A.3 for the list of pump models in the database). When simulating pump operation, the water reservoir and suction pipe geometries are used to ensure that the net positive suction head required (NPSHr) by the pump is less than the calculated net positive suction head available (NPSHa) [35]. This ensures that cavitation will not occur during pump operation [34]. The cost of specific pump models, when known, are included in the pump database. Otherwise, the pump cost is assumed to scale linearly with the maximum pump operating power. The pump module passes the cost and required pumping power of each feasible pump into the power system module and operation simulation.

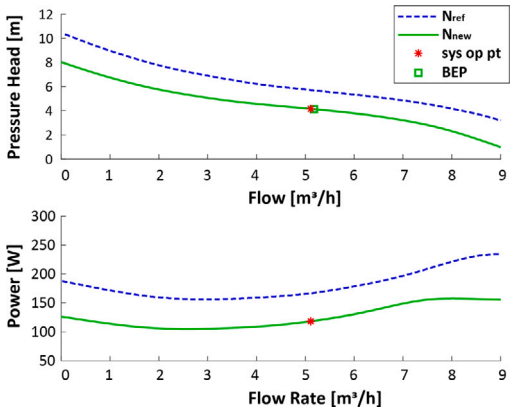

Fig. 4. A visualization of how the pump operating point and pumping power are identified using the affinity laws. The system flow rate, Q_{sys}, is used to select a set of feasible pumps from the database such that the system flow rate is within 70%–120% of the pump BEP flow rate (square). Each pump is assumed to be paired with a motor driver that can be used to shift the characteristic curves, expanding the pump operating range. The affinity laws are used to determine the desired characteristic curves (solid line) that intersect with the system operating point (asterisk) based on the reference curves (dotted line).

2.2.4. Power system module

The power system module sets up the calculation of the power available, P_{avail}, to the rest of the system by calculating the power output from a unit panel area, P_{PV}, based on the local weather. The power system includes solar panels with energy storage options of batteries and/ or a water storage tank. P_{PV} is calculated using a method called the modified single-diode model (summarized in the SI Section 2) [36]. The modified single-diode model allows for the calculation of the current–voltage curve for all temperatures and irradiances. The P_{PV} for each temperature and irradiance condition is calculated as

$$P_{PV} = \max(I\,V)/A_{panel}, \tag{11}$$

where $\max(I\,V)$ is the maximum power point (MPP) [W] of the current–voltage curve and A_{panel} is the area of a single solar panel [m^2], given by the panel manufacturer datasheet. Using the MPP assumes that the system has maximum power point tracking (MPPT) capabilities. Calculating P_{PV} as varying with the local weather conditions allows SDrOP to simulate operation and energy flow throughout the season and produce a location-specific power availability profile for the system.

2.2.5. Operation simulation

The operation simulation is a logic loop that calculates where energy and water will flow for each time step of the irrigation season. This allows for the performance of a design to be evaluated in terms of how much of the crop water demand it can deliver. There are four different energy paths that can be taken to deliver water to the crops and two paths to store energy. These six paths are illustrated in Fig. 5(a).

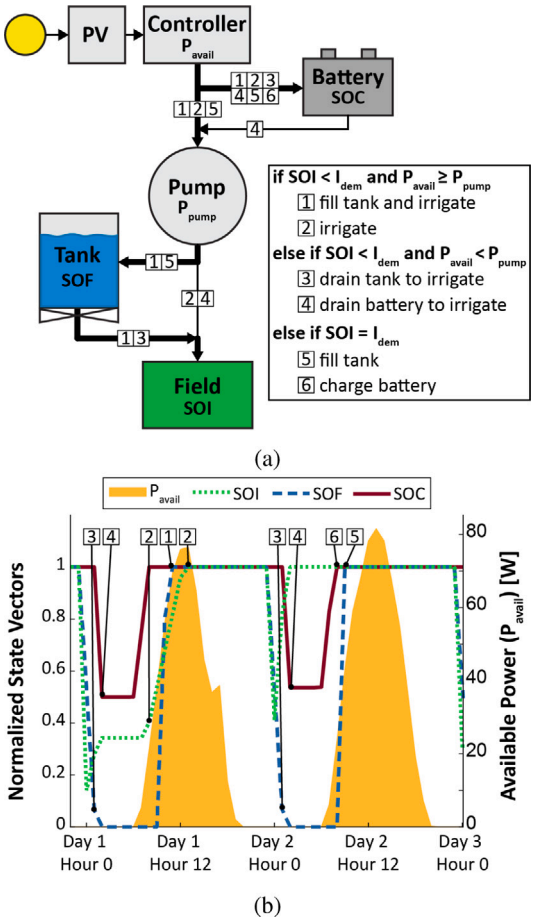

Fig. 5. An illustration of the logic flow loop and representation of the simulated system operation. In **(a)** the energy and water flow diagram is shown. There are six flow paths of energy connecting the photovoltaic (PV) system (power, P_{PV}), controller (power, P_{avail}), battery, pump (power, P_{pump}), water storage tank, and field. The arrowed connections corresponding to each of the energy paths are designated by numbers 1–6 (e.g., the first path is made up of all the connections labeled with a 1 and path 1 is bolded as an example). As described in the boxed conditional statement, flow paths are checked in numbered order at each time step and activated based on the weather-dependent available power (P_{avail}) and the state of the battery, tank, and irrigation of the field, designated as the state of charge (SOC), state of fill (SOF), state of irrigation (SOI), and irrigation demand (I_{dem}). In **(b)** the power values and normalized SOC, SOF, and SOI for two days of operation on a representative small field illustrate the conditions under which each flow path might be activated.

Within the logic loop the irrigation demand, or the amount of water the irrigation system must deliver to meet the crop water demand, is calculated at the start of each day in m^3 by rearranging the soil water balance defined in the FAO Irrigation and Drainage Paper No. 56 [25] as

$$I_{dem,n} = f_w A_{field}(D_{r,n-1} - Pr_n + RO_n - RAW_n + ET_{c,n})/1000. \quad (12)$$

Here, the soil water level is set to the minimum needed to not stress the crop ($D_{r,n} = RAW_n$), n is the day of the irrigation season, D_r is the water lost to the root zone of the crop, or the root zone depletion [mm], Pr is precipitation [mm], RO is runoff [mm], f_w is the soil wetted fraction (which is set to 0.3 for drip irrigation [25]), and A_{field} is the field area [m^2]. RAW is the readily available water [mm], or the amount of water in the root zone that the plant can uptake most efficiently. This soil water balance assumes a deep groundwater table, so there is no capillary rise, it neglects deep percolation, and $I_{dem,n}$ is calculated such that the $D_{r,n}$ is at RAW_n and $D_{r,n-1}$ is at the $D_{r,n}$ of the previous day. RAW_n is defined as

$$RAW_n = d_n TAW, \quad (13)$$

where TAW is the total available water that the crop can extract from the soil [mm], a constant that depends on the depth of the crop roots and soil properties defined in the Case Definition. The depletion fraction on day n, d_n, is calculated by adjusting for daily ET_c as defined in Table 22 of [25].

$$d_n = d_{const} + 0.04\,(5 - ET_{c,n}), \quad (14)$$

where d_{const} is the constant crop dependant depletion fraction assuming $ET_c = 5$ mm/day.

The available power is calculated throughout the day as

$$P_{avail,i} = P_{PV,i}\,\eta_{MPPT}\,\eta_{conv}\,A_{PV}, \quad (15)$$

where i is the sub-daily time interval indices (dependent on the resolution of the input weather data), $\eta_{MPPT} = 98\%$ and $\eta_{conv} = 95\%$ are the assumed efficiencies for the MPPT unit and the electrical converter, and A_{PV} is the solar panel area for the system design [m^2].

$P_{avail,i}$ can go towards charging the battery or powering the pump (P_{pump}), and water from the pump can go towards filling the tank or irrigating the crops on the field. State vectors, namely the state of charge (SOC) of the battery [Wh], state of fill (SOF) of the tank [m^3], and state of irrigation (SOI) of the field [m^3], are calculated in the operation logic loop to keep track of where energy and water are used or stored at each time interval.

Before the irrigation demand is met, the time remaining to irrigate [s], t_{ri}, is calculated as

$$t_{ri,i} = min\left(\frac{I_{dem,n} - SOI_{i-1}}{Q_{sys}}, \Delta t\right), \quad (16)$$

where Δt is the time interval. The calculation of t_{ri}, and other time variables, allows for other paths to be used during the same time step once a state vector is filled. Note that SOI is initialized at zero and is set to zero at the start of each day.

The conditions required to select each flow path are checked in order, following a fixed operation priority as depicted in the boxed conditional statement in Fig. 5(a). If the irrigation demand has not been met, the first check is if there is enough $P_{avail,i}$ to deliver water through path 1. Path 1 fills the tank and irrigates at the same time. During this path, the time to fill the tank, t_{tf} [s], is calculated as

$$t_{tf,i} = \min\left(\frac{C_{tank} - SOF_{i-1}}{Q_{tank,i} - Q_{sys}}, t_{ri,i}\right), \quad (17)$$

where C_{tank} is the tank capacity [m^3] and Q_{tank} is the flow rate from the pump going into the tank [m^3/s] (details of the tank flow rate calculation are provided in the SI Section 3). The state equations for path 1 are

$$SOI_i = SOI_{i-1} + Q_{sys}\,t_{ri,i}, \quad (18)$$

$$SOF_i = SOF_{i-1} + (Q_{tank,i} - Q_{sys})\,t_{tf,i}, \quad (19)$$

and

$$SOC_i = SOC_{i-1} + (P_{avail,i} - P_{pump,i})\,t_{tf,i}. \quad (20)$$

Fig. 5(b) illustrates the relative state of $P_{avail,i}$, SOC, SOF, and SOI corresponding to each of the flow paths over a period of two days. For example, path 1 is selected mid-way through day one when there is sufficient $P_{avail,i}$, $SOF < 1$, and $SOI < 1$.

If there is not enough $P_{avail,i}$ to complete path 1, the next check is if there is enough $P_{avail,i}$ to irrigate the field directly through path 2. The state equations for path 2 are Eq. (18), as well as

$$SOF_i = SOF_{t-1} \quad (21)$$

and

$$SOC_i = SOC_{i-1} + (P_{avail,i} - P_{pump})\, t_{ri,i}. \tag{22}$$

If there is not enough P_{avail} for path 1 or 2, there is not enough power from the panels to directly deliver water to the field. If the irrigation demand is still not met, the tank and the battery storage are checked. The time to drain the tank, t_{tdt} [s], and the time to drain battery, t_{tdb} [s], are calculated as

$$t_{tdt,i} = min\left(\frac{0 - SOF_{i-1}}{Q_{tank,i} - Q_{sys}}, t_{ri,i}\right) \tag{23}$$

and

$$t_{tdb,i} = min\left(\frac{0.5C_{batt} - SOC_{i-1}}{P_{avail,i} - P_{pump,i}/\eta_{batt}}, t_{ri,i}\right), \tag{24}$$

where C_{batt} is the battery capacity [J], $\eta_{batt} = 85\%$ is the assumed battery efficiency, and the maximum depth of discharge for the battery is set to 50%. If the tank or battery are already at their minimum capacities then t_{tdt} and t_{tdb} are zero and pathways 3 and 4 are not used.

If there is enough water stored in the tank, path 3 is used with the state equations

$$SOI_i = SOI_{i-1} + Q_{sys}\, t_{tdt,i}, \tag{25}$$

$$SOF_i = SOF_{i-1} - Q_{sys}\, t_{tdt,i}, \tag{26}$$

and

$$SOC_i = SOC_{i-1} + P_{avail,i}\, t_{tdt,i}. \tag{27}$$

If there is enough energy stored in the battery, path 4 is used with state equations including Eq. (21), as well as

$$SOI_i = SOI_{i-1} + Q_{sys}\, t_{tdb} \tag{28}$$

and

$$SOC_i = SOC_{i-1} + (P_{avail,i} - P_{pump}/\eta_{batt})\, t_{tdb}. \tag{29}$$

If there is not enough power or energy storage to run the other paths, or the irrigation demand for the day has already been met, the SOI_i is set to SOI_{i-1}. The loop checks if the tank and battery are full, and if not, it tries to fill them using paths 5 and 6, respectively. For path 5, the t_{tf} is updated as

$$t_{tf} = min\left(\frac{C_{tank} - SOF_{i-1}}{Q_{tank,i}}, \Delta t\right). \tag{30}$$

The state equations to fill the tank for path 5 are

$$SOF_i = SOF_{i-1} + Q_{tank,i}\, t_{tf} \tag{31}$$

and

$$SOC_i = SOC_{i-1} + (P_{avail,i} - P_{tank,i})\, t_{tf}. \tag{32}$$

The system uses any remaining power to charge the battery through path 6. The state equations are Eq. (21) and

$$SOC_i = SOC_{i-1} + P_{avail,i}\, \Delta t. \tag{33}$$

For all the paths, any extra power is used to charge the battery until the battery is fully charged. If there is any extra power after path 6 and the battery is fully charged, the power is unused.

The operation is defined such that any energy storage is drained to irrigate at the start of each day and later filled when there is enough solar energy available. For example, in Fig. 5(b) at the start of both days the irrigation demand has not been met but there is no solar power available yet, so paths 3 and 4 are used to irrigate, draining the energy storage. Towards the middle of each day, once there is enough P_{avail}, the simulation uses paths 1 and 2 to irrigate and fill the energy storage if the irrigation demand has not yet been met (day one) or it uses paths 5 and 6 to fill the energy storage if the irrigation demand has already been met (day two).

At the end of each day, the daily amount of irrigation that has been delivered [m^3] by the system, I_{del}, is determined as

$$I_{del,n} = SOI_{i,end}, \tag{34}$$

where i, end is the last time interval of the day. The adjusted crop evapotranspiration, ET_a, in mm and D_r are calculated at the end of the day as

$$ET_{a,n} = K_{s,n}\, ET_{c,n} \tag{35}$$

and

$$D_{r,n} = D_{r,n-1} - Pr_n + RO_n - I_{del,n} + ET_{a,n}, \tag{36}$$

where D_r is constrained such that $0 \le D_{r,n} \le TAW$ and K_s is the water stress coefficient which accounts for the water stress felt by the crop. If D_r is less than or equal to RAW, then $K_s = 1$. If the D_r is greater than RAW, then K_s is calculated as

$$K_{s,n} = \frac{TAW - D_{r,n}}{(1 - d_n)\, TAW}. \tag{37}$$

The operation simulation defines the relationship between the crop irrigation demand and the irrigation that can be delivered by the specified system design. The system performance affects crop water stress through ET_a, and in turn the crop growth and yield, as well as the system reliability.

2.2.6. Crop yield module

The yield module determines the crop yield and revenue for the given case definition based on the amount of water the system is able to deliver. The yield is calculated by assuming a relationship between yield and crop water use and adjusting the maximum crop yield, Y_m, based on that relationship. Y_m is calculated using the agro-ecological zone method following FAO Irrigation and Drainage Paper No. 33 [37], which assumes the crop experiences no water stress, no fertilizer stress, negligible soil salinity and acidity, and no pest conditions. The adjusted yield, Y_a, is derived from an empirical yield versus evapotranspiration curve [38,39],

$$\frac{Y_a}{Y_m} = Y_{rel}\left(\frac{\sum_{n=1}^{n_{tot}} ET_{a,n}}{\sum_{n=1}^{n_{tot}} ET_{c,n}}\right)/100, \tag{38}$$

where Y_{rel} is the yield-curve that relates relative percent yield to relative percent crop evapotranspiration, and n_{tot} is the total number of days in the irrigation season.

Fig. 6 shows the Y_{rel} curve for olives, which are used in this study. The curve depicts the drought resistant nature of the olive crop as it stays at or above 100%[2] yield for 85% or greater relative crop evapotranspiration, corresponding to an average water stress, K_s, less than 0.15. The parabolic shape of the curve shows that small reductions in evapotranspiration, related to reductions in irrigation, cause an almost undetectable reduction in yield, implying an irrigation scheme that does not meet 100% of the crop water demand could be used in the design process. The curve is based on the olive cultivar variety Picual in Cordoba, Spain, but was compared to other varieties and locations and found to fall within the margins of error. For crops that do not have an empirically derived yield versus evapotranspiration curve, a yield response to evapotranspiration equation is used to calculate Y_a (detailed in the SI Section 4) [37].

[2] Multiple years of data with full water application were collected, and the average of those years was selected as the 100% yield case, but there were some water applications that went above this average 100% yield value.

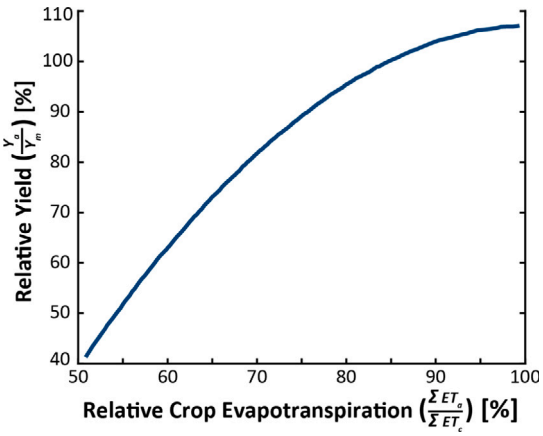

Fig. 6. The empirical yield curve for olives. The curve show the percent change in yield as a function of the change in crop evapotranspiration. Olives are shown to be water stress resistant crops: a small decrease in relative evapotranspiration causes negligible change in the yield.

2.3. Design optimization

The goal of the optimization is to produce a location-specific, low-cost design for the given case definition. The optimization loop iterates through permutations of pumps and power system capacities (Fig. 2), simulating the performance of each proposed design as described in Section 2.2.5. The performance of a design is characterized by the reliability with which it can meet the crop water demand over the season. The LCC of the design is computed using location-specific cost data, and the revenue from the crop yield is used to determined the lifetime profit. For the sake of computational efficiency, it is assumed that one season is representative of all crop seasons over the course of the system lifetime. The objective of the optimization can be set to either minimize the LCC or maximize the lifetime profit. The design variables are the pump, solar panel area, tank capacity, and battery capacity.

The LCC model includes the LCC of each component, including the hydraulic network components, which do not vary in the optimization. The component costs are based on local contractor and equipment prices from the given location. For this study, the cost data were collected from economic reports, compiled by local research partners, and from contractor invoices for solar-powered drip systems installed in Morocco [10]. Detailed component costs are included in Appendix A.1. The local crop prices were collected from FAOSTAT [40].

The cost objective function is defined as

$$\boldsymbol{min}\ LCC = \sum_r (1+k_i) IC_r + MC_r + RC_r\ , \tag{39}$$

where

$$IC_r = UC_r\ C_r\ , \tag{40}$$

$$MC_r = \begin{cases} k_{m,r}\ IC_r \left(\frac{1+FR}{IR-FR}\right)\left(1-\left(\frac{1+FR}{1+IR}\right)^{LT}\right) & \text{if } IR \neq FR \\ k_{m,r}\ IC_r\ LT & \text{if } IR = FR \end{cases} \tag{41}$$

and

$$RC_r = IC_r \sum_{j=1}^{M_r} \left(\frac{1+FR}{1+IR}\right)^{\left(\frac{LT\,j}{M_r+1}\right)}\ . \tag{42}$$

Here, IC_r, MC_r, and RC_r, are the initial cost and the net present value maintenance and replacement costs over the system lifetime [USD] of the rth component. These equations are consistent with LCC models used for similar systems [21,22]. The initial cost of the rth component is computed as the unit cost, UC_r, multiplied by the component capacity, C_r (Eq. (40)). The installation cost is computed as a fraction of the initial system cost using the installation cost coefficient, k_i. The maintenance cost is computed as a fraction of the initial cost (Eq. (41)) using the maintenance cost coefficient of the rth component, $k_{m,r}$. These cost coefficients are based on cost data collected from local contractor invoices (values provided in Appendix A.1). Inflation rate, FR, and interest rate, IR, are both constants provided in [22]. The system lifetime, LT, is set to be 20 years, which is the expected lifetime of the solar panels. Each component has a specified number of replacements within that lifetime, M_r, which are shown in Table 1. The panels are assigned a 10% area replacement after 10 years to simulate panel efficiency degradation. The component lifetimes and replacement frequency were based on manufacturer recommendations. The cost of each replacement is calculated in Eq. (42) using the replacement number counting index j. A more detailed description of the calculation of each component cost is presented in [41,42].

Table 1
Component lifetime and number of replacements over 20-year system lifetime.

Component	Lifetime [yrs]	Replacement number
PV panels	20	1 (10%)[a]
Battery	2	9
Tank	25	0
Pump	5	3
Laterals and emitters	10	1
Additional hydraulic components[b]	20	0

[a]Solar panel lifetime is set to 20 years, but 10% of panel area is replaced after 10 years to simulate panel degradation.
[b]Includes main, submain, pipe fittings, filters, and fertigation unit.

The profit objective function is defined as

$$\boldsymbol{max}\ Profit = Rev - LCC\ , \tag{43}$$

where

$$Rev = \begin{cases} Y_a\ A\ k_{cp} \left(\frac{1+FR}{IR-FR}\right)\left(1-\left(\frac{1+FR}{1+IR}\right)^{LT}\right) & \text{if } IR \neq FR \\ Y_a\ A_{field}\ k_{cp}\ LT & \text{if } IR = FR. \end{cases} \tag{44}$$

Eq. (44) defines the net present value revenue, where Y_a is the crop yield [kg/ha], A_{field} is the field area [ha], and k_{cp} is the crop price coefficient [USD/kg], which is a location-dependent constant [40].

The primary constraint in the optimization problem concerns the system reliability. The system reliability is defined as the loss of load probability (LLP) [22]

$$LLP = \frac{\sum I_{dem} - \sum I_{del}}{\sum I_{dem}}\ , \tag{45}$$

which is the fraction of the total irrigation demand that a design fails to meet over the course of a growing season. The cost optimization is subject to a minimum reliability constraint, $LLP \leq LLPT$, which means that the LLP for an optimal design cannot exceed a certain loss of load probability threshold (LLPT). An LLPT of 0 means that the design must meet the crop water demand with 100% reliability, and an LLPT of 1 means there is no reliability constraint imposed. A reduction in the system reliability will lead to a reduction in the water delivered by the system, which can increase the crop water stress and reduce the yield. Therefore, LLPT is proportional to the amount of crop water stress the designer is willing to tolerate based on agronomic considerations. For the profit optimization, the revenue from the crop yield depends on the amount of water the system delivers, so system reliability is intrinsic to the profit objective function.

Both the cost and profit optimization schemes are subject to bounds on the design variable capacities to ensure physically reasonable designs are produced. This includes a minimum panel area and, for any

Table 2
Baseline case definition.

Location	Marrakech, Morocco
Field area	1 ha
Weather data type, resolution	Typical meteorological year (TMY), hourly
Soil texture	clay loam
Crop	olive
Crop × Row spacing	5 m × 5 m
Pipe network inner diameters (main, submain, lateral)	83 mm, 59 mm, 16 mm
Emitter flow, activation pressure	8 Lph, 0.15 bar
Emitter type, number per crop	low-pressure PC, 2
Water source height/depth[a]	1 m
Loss of load probability threshold (LLPT)	0.15

[a]A positive value means the water source is located above the pump inlet.

design with non-zero tank and battery capacities, a minimum tank and battery capacity to avoid unrealistically small components. A maximum panel area, tank capacity, and battery capacity are set to reflect spacial and economic constraints of a small farm. In any design with a tank, the tank height is constrained by the head capacity of the selected pump to ensure that the pump is capable of filling its corresponding tank.

The optimization algorithm is a particle swarm optimization (PSO) [43]. The PSO framework was selected for its ability to handle discrete variables, such as the pump models in the pump database. A PSO is a heuristic algorithm in which a randomly generated set of solutions, or "swarm", iteratively propagates through the design space to converge on an optimal solution, while adhering to imposed constraints and algorithm parameters [44]. In this work, a solution to the optimization problem consists of a pump, panel area, tank capacity, and battery capacity, which together comprise a system design for the given case definition. While there is no way to mathematically guarantee that a heuristic algorithm converges on a global optimum, if the algorithm consistently converges on a solution after multiple runs of the same test case, this is a sufficient indication that the solution is optimal [44]. For the simulations presented here, the PSO swarm size was 20 and the convergence margin was 10 USD (see Appendix A.2 for all parameters). The algorithm parameters, such as the swarm size and convergence criterion, were selected based on tests of repeatable convergence for a range of drip system cases [41,42].

2.4. Baseline case

A one hectare olive orchard in Marrakech, Morocco was defined as a representative case and used for the analyses presented in this paper. Table 2 details this case definition, hereafter called the baseline case. Unless otherwise stated, the inputs used in SDrOP are those used in the baseline case.

The system operating point of the baseline case is a 5.1 m pressure head and a 6.9 m^3/h flow rate. The pump database and solar panel parameters are representative of locally-available pumps and panels. An LLPT of 0.15 was selected because olive trees are relatively water stress resistant, and can produce 100% yield with a relative evaporation of 85% (Fig. 6).

3. Optimization results and sensitivity analysis

3.1. Profit and cost optimization comparison

Although smallholder farmers are most sensitive to upfront cost, predicting the full financial commitment and profit generated by the drip systems can provide insight on impactful financing options, long-term affordability, and overall adoption of drip irrigation for farmers. To understand how the optimal system design and performance metrics of yield, LLP, and LCC change based on the optimization objective, systems designed by minimizing LCC were compared to systems designed by maximizing lifetime profit. The comparison is presented in Table 3. The analysis was conducted for seven field sizes, ranging from 0.25 to 2 ha. The same hydraulic layout was used for both optimization objectives, so the system hydraulic power and pump power for each field size are the same between the cost and profit optimizations.

Table 3
Profit- and cost-optimized design results for various field sizes.

	Field Area [ha]	0.125	0.25	0.5	0.75	1	1.5	2
	Hyd. Pwr. [W]	9	17	37	61	95	193	354
	Pump Max. Pwr. [W]	42	49	230	230	240	540	830
	Pump Pwr. [W]	29	46	74	118	180	295	636
Cost	PV Area [m^2]	0.30	0.49	0.80	1.28	1.91	3.18	6.80
	LLP	0.140	0.143	0.137	0.147	0.149	0.147	0.147
	LCC [10^3 USD]	0.887	1.426	2.601	3.700	4.861	7.658	10.901
	Yield [kg/ha]	9,926	9,925	9,926	9,924	9,924	9,924	9,924
Profit	PV Area [m^2]	0.34	0.55	0.97	1.54	2.29	3.56	7.65
	LLP	0.066	0.075	0.064	0.068	0.071	0.080	0.080
	LCC [10^3 USD]	0.919	1.479	2.680	3.827	5.058	7.974	11.312
	Yield [kg/ha]	9,944	9,942	9,945	9,944	9,943	9,940	9,940

The optimal power system design changed based on the optimization objective. In this analysis, energy storage options were never found to be optimal, but the optimal solar panel area is larger for profit-optimized systems. This means the cost-optimized designs are not able to deliver as much water as the profit-optimized designs, which can be seen in the larger LLP values and smaller yields for the cost-optimized systems compared to the profit optimized systems (Table 3). This indicates that the LLPT for the cost optimization imposes a less strict constraint on system reliability than the profit objective function. In other words, the profit optimization requires more reliable systems, and therefore larger and more expensive power systems. However, for the cases presented here, the difference in the results is small. The LCC for the cost-optimal systems is 3%–4% smaller than for the profit-optimal systems, and the increase in yield for the more reliable, profit-optimal systems is only 0.2% greater than for the cost-optimal systems. The relative LCC reduction provided by the cost optimization is an order of magnitude greater than the relative increase in yield provided by the profit optimization. Because the goal of this work is to reduce system cost to improve the accessibility of drip irrigation for smallholder farmers, the cost optimization was chosen over the profit optimization for subsequent analyses. The cost optimization is employed to analyze the sensitivity of the LCC to case definition inputs and the system reliability constraint.

3.2. Sensitivity analysis

SDrOP was used to explore the sensitivity of the optimal design LCC to field area, the reliability constraint, and weather variation. The goal of these sensitivity analyses is to gain insights on the implementation of solar-powered drip irrigation systems. The results have implications for optimal component selection, irrigation scheduling, system robustness to varying environmental factors, and the use of the low-pressure PC emitters.

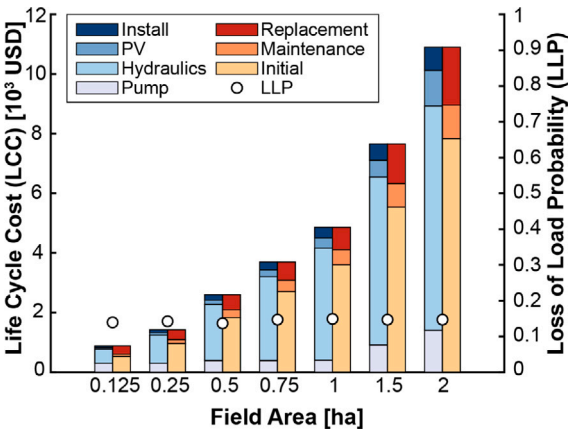

Fig. 7. The sensitivity of the optimum life cycle cost (LCC) to varying field area. For each field, the bars on the left break down the LCC into component costs. The bars on the right break down the LCC into initial, maintenance, and replacement costs. The loss of load probability (LLP) is plotted as circles with a right axis. The threshold (LLPT) was set to 0.15 for all cases.

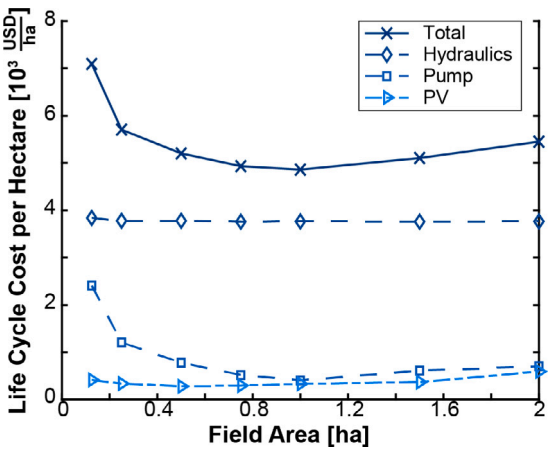

Fig. 8. The life cycle cost per hectare of cost-optimal systems for a range of field areas, broken up into components (hydraulics, pump, PV). Below the 1 ha case, the nonlinear behavior of the LCC per hectare curve is driven by the limited availability of pumps for low-pressure operating points. Above the 1 ha case, the nonlinearity is driven by the cubic scaling of hydraulic power with system flow rate.

3.2.1. Field area

The sensitivity of the optimal design to changes in field area was analyzed for the baseline case with field areas of 0.125–2 ha. Fig. 7 shows the resulting optimal design LCCs, broken down by component costs and initial, maintenance, and replacement cost. The LLP is plotted for each design, indicating its seasonal reliability. The pump and solar panel details for each design are shown in Table 3.

For all field areas, the hydraulic network is the largest component cost, the initial cost makes up the majority of the LCC, and all of the optimal designs are direct-drive systems without energy storage (Fig. 7). The hydraulics contribute between 54%–77% of the LCC for all cases. The initial cost accounts for 50–70% of the LCC. The replacement cost, which includes hydraulic, solar panel, and pump replacements over the system lifetime, was higher than the maintenance cost across field areas. The maintenance costs are sensitive to the local labor costs, which tend to be low in Morocco [10]. For all of the field areas, the LLP is just below 0.15, indicating that approaching the LLPT reduces the LCC, as expected. The fact that the LLP of the designs does not exactly reach the LLPT suggests that the marginal reduction in LCC gained by slightly increasing LLP to match LLPT is too small to result in further iterations before the solution converges.

Fig. 8 presents the LCC per hectare as well as the hydraulic, pump, and panel cost per hectare for each field area. The plot shows that LCC per hectare is nonlinear with field area. The LCC per hectare decreases with increasing field area, until it reaches a minimum at one hectare, and then increases with increasing field area. The hydraulic cost per hectare remains relatively constant with field area, and therefore does not contribute to the nonlinear behavior of the LCC per hectare curve.

The LCC per hectare relationship with field area has two distinct regions. The first is an economies of scale region leading up to the one hectare case that is driven by the per hectare cost of the pump and power system (Fig. 8). A similar pump model was selected for systems on the smaller fields, as indicated by maximum pump power (Table 3), namely for the 0.125 ha and 0.25 ha cases, and for the 0.5, 0.75 and 1 ha cases. The smaller systems used similar pumps because the novel, low-pressure PC emitters resulted in drip system designs with relatively low-pressure, high-flow rate operating points. These operating points are not typically within the PORs of existing centrifugal pumps, but the motor driver expands the operating range of the pumps to accommodate these abnormal operating points. Therefore, the optimal designs for the smaller fields share pump architectures. It became evident, while populating the pump database and surveying pump catalogs of local Moroccan distributors, that there is a lack of low-cost pumps that can operate efficiently at these points. Pumps selected for smaller fields will be oversized, and therefore overpriced, and could potentially degrade more quickly if they are primarily operated outside their POR. This indicates a possible gap in the local pump market for the small farm irrigation using low-pressure drip emitters.

The second region of the LCC per hectare plot is the diseconomies of scale region that begins above one hectare. In this region, fluid mechanics drives the diseconomies of scale as field area increases. For all cases, it is assumed that the entire field is irrigated at once, which means that the system flow rate increases with field area. This leads to an increased pressure drop because pipe frictional losses scale with the flow rate squared. Hydraulic power is the product of flow rate and pressure, so the hydraulic power scales with the cube of the flow rate. As such, the power system capacity and cost increase with increasing field area. Additionally, when pump costs were unknown, it was assumed that the pump cost scaled linearly with pump power. Therefore, the strong scaling relationship between operating power and flow rate is magnified by the pump cost for field areas larger than one hectare.

3.2.2. Reliability constraint

The sensitivity of the optimal LCC to LLPT was analyzed, and it was shown that small adjustments in the reliability constraint can lead to a significant reduction in the system LCC. Fig. 9(a) shows that LCC drops precipitously (by 25%–49%) between LLPT values of 0 to 0.1 and remains relatively constant between 0.1 and the maximum LLPT. This means that a 10% relaxation of the reliability constraint significantly reduces the optimal system cost. The large cost reduction comes from a change in the selected components: optimal systems for which the LLPT is 0 all incorporate energy storage, whereas for an LLPT of 0.1 or higher, all the optimal systems are direct-drive. Requiring high reliability (LLPT = 0) forces the system to meet spikes in the irrigation demand (Fig. 9(b)). To meet this demand in full, a large solar array or energy storage capacity is required, which significantly increases the system cost. The fact that energy storage is required in the optimal design when LLPT is 0 means the optimization found it was less expensive to meet the additional irrigation demand with energy storage than by solely increasing the solar panel area. Increasing the LLPT from 0 to 0.1 meant that the system no longer had to meet the large spikes in irrigation demand (Fig. 9(b)), and therefore, the optimal design had a less expensive, direct-drive power system.

The shape of the LLPT sensitivity plot illustrates how relaxing the reliability constraint affects the daily irrigation demand. The initial steep decrease in power system capacity and LCC is the result of increasing

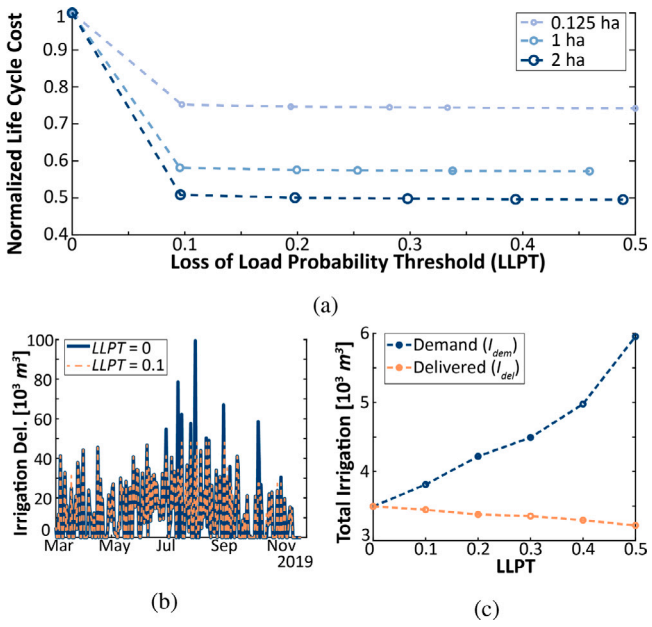

Fig. 9. Sensitivity of the LCC of the cost-optimal design to the reliability constraint: **(a)** demonstrates the normalized LCC as a function of the loss of load probability threshold (LLPT) for the baseline case with field areas of 0.125, 1, and 2 ha — the LCC for each field area is normalized to the LLPT = 0 case; **(b)** shows the water delivered over the season for the baseline case with an LLPT of 0 and 0.1; and **(c)** demonstrates the change in total irrigation demand and water delivered for the cost-optimal designs with varying LLPT.

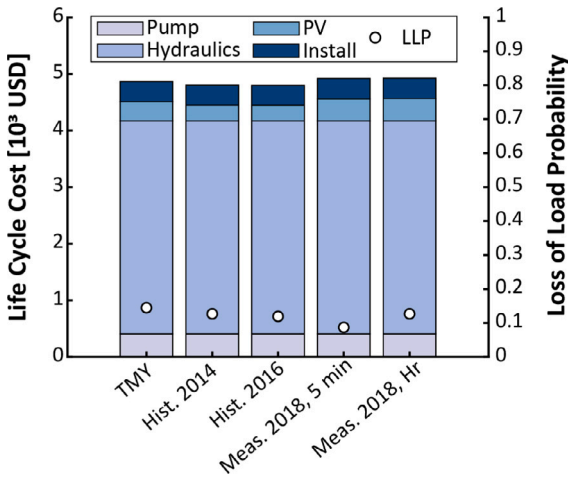

Fig. 10. The sensitivity of the optimal LCC to varying weather conditions for the baseline case. The stacked bar is LCC broken into component costs. The typical meteorological year (TMY) data for weather used in the baseline case was compared to historical data from 2014 and 2016 (both drought years in Morocco) as well as measured data from 2018. All of the datasets had hourly resolution, except the measured data, which was taken at both five-minute and hourly intervals.

LLPT from 0 to 0.1, which alleviates the requirement that the system meet the high-demand days. However, as LLPT is increased further, irrigation demand also increases (Fig. 9(c)); if the full irrigation demand is not met by the system at the end of one day, the irrigation demand on the following day will be higher. This is because the soil water balance calculation uses the water level from the previous day. Therefore, if the irrigation demand is not met, the soil will be drier, requiring more water to achieve the correct saturation in the root zone (Eq. (12) and (36)). In other words, the daily irrigation demand compounds every time the system fails to deliver enough water to the crops. This results in the leveling off of the optimal system LCC with increasing LLPT (Fig. 9(a)), which indicates that increasing the LLPT above 0.1 results in diminishing returns for minimizing the LCC. The curves illustrate the trade-off between reducing the irrigation delivered – which enables a smaller power system capacity with a lower LCC – and increasing irrigation demand – which requires a larger power system capacity with a higher LCC. Because the irrigation demand increases as the reliability requirement relaxes, the power system capacity cannot decrease as steeply past a certain point (Fig. 9(c)).

The point of greatest return on the LLPT sensitivity plot is the point where the steep decrease in LCC meets the plateau (Fig. 9(a)). The location of this point on the plot is directly determined by the case definition parameters, namely the selected crop, local weather patterns, soil properties, and the field area. The water stress resistance of the crop, the soil mechanics, and the weather over the growing season will determine how much the LLPT can be increased without impacting the crop yield. Therefore, the selected crop and location will influence the horizontal position of the point of greatest return on the plot. The field area and local weather patterns will determine the relative magnitude of possible cost savings. As shown in Fig. 9(a), the magnitude of the LCC reduction is greater for larger fields. This is because the power requirement scales nonlinearly with field area (Section 3.2.1). In addition, the local weather patterns will dictate the availability of solar irradiance, which will influence the power system capacity. If the availability of solar irradiance for the given location is low or highly variable, the optimal power system capacity must remain large to consistently provide enough power. In these cases, the opportunity for LCC reduction by increasing LLPT will be diminished. As such, the field area and local weather will influence the vertical location of the point of greatest return on the plot.

3.2.3. Weather variation

SDrOP was used to determine the sensitivity of the cost-optimal designs to variations in local weather patterns (Fig. 10). For this analysis, it is assumed that the yearly weather is known a priori and that it remains unchanged for the 20-year lifetime of the system.

The baseline case was run with the TMY data and compared to historical weather data taken from a National Institute for Agricultural Research (INRA) station in Marrakesh, Morocco in 2014 and 2016 and measured data from a Moroccan field trial site 2 km away from the INRA station in 2018 [18]. The 2014 and 2016 data were included because Morocco experienced a drought in both years [45,46]. Fig. 10 shows the LCC of the optimal designs produced using each weather dataset. Only the size of the solar panels changes across designs. The change in the LCC of the cost-optimal designs to the weather input changes are small, ±1% compared to the TMY data case, implying that the optimal designs produced by SDrOP are robust to weather variations for the baseline case. The datasets used in this analysis varied from the TMY data: average irradiance varied by +6%/−9%, average ET_0 varied by −23%, and total precipitation varied by +3%/−29% (shown in the SI Section 5). The TMY data [26] and INRA historical weather data have hourly resolutions, and the measured data has hourly and five-minute resolutions.

The optimal design produced when using the measured, five-minute resolution data has a slightly lower LLP than the design produced with the measured, hourly resolution data. This means that the former is more reliable than the latter, suggesting that using higher resolution weather data produces a system design that can better meet fluctuations in the irrigation demand over the season. However, this slight increase in reliability corresponds to a negligible change in the optimal LCC between the two designs, indicating that there is not a meaningful difference in the cost-optimum when using weather data with five-minute or hourly resolution. Given that globally available weather data often has hourly resolution [26], these results indicate that hourly weather data is sufficient for cases with similar crops and local weather patterns to the baseline case.

Table 4
Benchmark comparison of system designs produced by SDrOP and compass.

	Life Cycle Cost (LCC) [10^3 USD]	LCC Saving [%]	PV Area [m^2]	Irrigation [m^3/year]
Compass	8.86	–	4.83	2970
SDrOP, LLPT = 0	5.63	36	1.73	1812
SDrOP, LLPT = 0.15	3.90	56	0.67	1778

4. SDrOP model benchmarking

The SDrOP optimal design was benchmarked against a design produced by commercial software, and against the field performance data of a small-scale, solar-powered drip system in Morocco. For both analyses, the benchmarking case was a 0.52 ha olive orchard in Marrakech, Morocco.

4.1. Commercial benchmark

Two solar-powered drip system designs produced by SDrOP, for an LLPT of 0 and 0.15, were compared to the designs produced by a commercial software package. The Lorentz software package, Compass [14], was chosen as the commercial software benchmark because it has a similar architecture to SDrOP. Compass sizes solar-powered pumping systems based on an input location and average water demand. Table 4 compares the PV panel area, LCC, and total volume of water delivered for the designs produced by Compass and SDrOP. The LCC of the SDrOP optimal designs are 36% and 56% lower than the Compass designs for an LLPT of 0 and 0.15, respectively.

The cost reduction between the SDrOP and Compass designs is due to the component sizing. SDrOP produced designs with a solar panel area that is up to 86% smaller than the Compass result. Additionally, the Lorentz pump selected by Compass is more expensive than the locally-available pumps selected by SDrOP. This is because the Compass pump database is restricted to Lorentz pumps. Compass selected a 700 W pump (Lorentz CS-F4-3) for a drip system with an operating power of 120 W [18]; this pump is significantly larger and 73% more expensive than the pump selected by SDrOP.

SDrOP is able to design significantly less expensive systems than Compass because it uses higher resolution inputs and captures subsystem interactions. Compass takes in a single value for required water volume, so the yearly irrigation amount is calculated by multiplying the average daily water demand by the number of irrigation days in the season. Compass then uses local, average monthly irriadiance data to determine available power. In SDrOP, the daily crop irrigation demand is calculated within the operation simulation using daily weather data and simulated soil water balance dynamics. As a result, the total irrigation volume calculated by Compass is larger than that computed by SDrOP (Table 4).

The SDrOP reliability constraint adds modeling flexibility compared to the Compass software. As shown in Section 3.2.1, varying LLPT can lead to further system cost savings. For the case with an LLPT of 0, the optimal design has a higher LCC than the optimal design for an LLPT of 0.15. This is because the latter requires a larger panel area and energy storage capacity to meet the crop water demand on days with low solar irradiance. When the reliability constraint is relaxed (LLPT = 0.15), the design does not include energy storage components, so the optimal power system capacity is reduced, and therefore, less expensive. Increasing the input data resolution and modeling system performance in detail enables SDrOP to select appropriately-sized pumps and design power systems with the minimum required capacity for drip irrigation applications. As a result, SDrOP is able to produce designs that are significantly less expensive than those produced with the commercial software benchmark.

4.2. Experimental benchmark

The simulated performance of the SDrOP optimal design was benchmarked against operational data from an existing small-scale, solar-powered drip system. The goal of this comparison was to determine if the optimal design produced by SDrOP using TMY weather data was a physically feasible design.

4.2.1. Experimental and analytical methods

A solar-powered drip irrigation system was installed in Marrakech, Morocco to collect operational data for a small-scale system. The data from this field trial were used, in part, to create SDrOP, and as such, the installed power system was not an optimal design. The field site was a 0.52 ha olive orchard at an agricultural research site operated by the International Center for Agricultural Research in the Dry Areas (ICARDA) and INRA. A hydraulic network of the low-pressure PC emitters, filters, and a fertilizer unit were installed on the field. The pipe layout was based on the preexisting crop layout. Pressure sensors (Lorentz LPS-500, SSIP51-15-G-UC-I36-20MA) and a flow meter (Dwyer WMT2-A-C-07-10) were installed in the hydraulic network. Solar panels (CS6P-270Wp), a surface centrifugal pump (Lorentz CS-F4-3), and a solar pump controller (Lorentz PS2-600) with integrated MPPT and datalogging capabilities were installed. The controller recorded sensor data, pump shut-off instances, and the electrical power consumed by the pump motor. The controller collected data at 10-minute intervals, and a Lorentz PS 3G communicator sent the data to a server via the local cellular network. A weather station (HOBO U30-NRC) was also installed on site to measure irradiance (HOBOS-LIB-M003), precipitation (Davis S-RGF-M002), temperature and relative humidity (HOBO S-THB-M008), and wind velocity (Davis S-WCF-M003). The data were recorded with 5-minute resolution and stored locally on the device. The specific setup, operation, and maintenance procedures for the field trial are described further in [18].

The system operating point (pressure and flow rate), pump electrical power consumption, and local weather data were recorded from May 2018 to April 2019. The data were filtered to remove any excessively high flow rate and pressure points outside the expected flow rate and pressure range for the hydraulic system. These outliers can be attributed to erroneous sensor measurements and a few instances of leaks or closed valves during system operation. Previous analysis of the system operation data validated that the SDrOP hydraulics module (Section 2.2.2) could accurately predict the behavior of a given drip system hydraulic layout [18]. Insights gained during the implementation of this field trial were used to identify the architecture and capability requirements that led to the creation of the SDrOP model theory presented in Section 2. These requirements are described in detail in [18].

SDrOP was then used to produce a cost-optimized design for the benchmarking case, which was the same size as the field trial system. The irrigation schedule used during the field trial, which was computed by on-site agronomists, was input to the agronomy module as the desired irrigation schedule. SDrOP uses TMY weather data, which means the optimal design was produced without a priori knowledge of the actual weather in the field. To determine how the optimal design would have performed in the field, the modified single-diode model (Section 2.2.4) was used to predict the power output of the optimal design given the measured on-site weather data from the field trial. The predicted power output of the optimal design was compared to the pump power consumption measured during the field trial.

4.2.2. Comparing measured power consumption to predicted optimal design performance

The power comparison between the predicted optimal design performance and the measured pump power consumption is shown in Fig. 11. The optimal design has a direct-drive power system with a panel capacity of 0.27 kWp (peak power production at Standard Testing

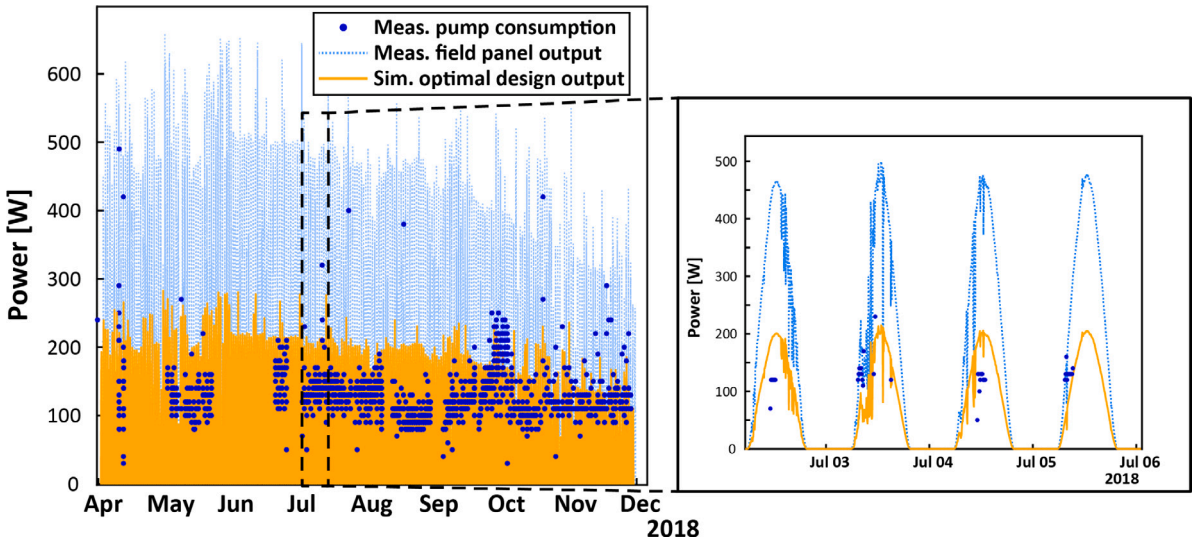

Fig. 11. The power output of the installed panels (dotted line), the measured pump power consumption (circles), and the predicted power output of the optimal design simulated using measured, on-site weather data (solid line) are shown. The optimal panel area is smaller than the installed panel area, but the simulated power output of the optimal panel capacity exceeds the measured power consumption for 92% of the pump operating points. This indicates that the installed power system was oversized, allowing irrigation to start earlier in the day, but that the optimal design would have been able to provide enough power to operate the field system.

Conditions [47]) and an LCC of 3900 USD. The predicted output of the optimal panel capacity exceeds the measured power consumption for the majority of the pump operating points. Over the course of the field trial, 92% of the pump operating points fall within the predicted power production range of the optimal design, indicating that the optimal power system would have been able to operate the installed system with less than 10% failed irrigation events. These results show that the optimal design would have been able to reliably operate the field system in the on-site weather conditions from May 2018 to April 2019.

The data also show that the measured power output of the installed panels was always greater than the predicted power output of the optimal panel capacity and the measured pump power consumption; this means that the installed panel capacity was oversized for this field. The inset of Fig. 11 shows that some of the pump operating points are inside the power production range of the installed system, but horizontally outside of the predicted power production range of the optimal design. The installed panel capacity enabled irrigation to start earlier in the day – when solar irradiance was lower – than the optimal panel capacity would have because the installed system was oversized. However, the optimal system would have provided enough power for these irrigation events, starting later in the day. As such, the pump operating points that are horizontally outside the optimal predicted power production are still counted as being within range for the optimal system.

5. Discussion

The sensitivity analyses and benchmarking results presented in this paper demonstrate how location-specific case parameters influence a cost-optimal drip system design. These results also illustrate how gaps in available software tools and local component availability impact the design space. Although this paper focuses on a specific case study, the analytical insights can be applied more generally as guidelines for designing and operating low-cost, solar-powered drip systems, which may be of interest to irrigation engineers and researchers globally. In addition, the modular SDrOP architecture makes it easy to adapt for a broader range of case studies.

5.1. Sensitivity analysis

This work presented several sensitivity analyses that can be used to inform system cost reduction and the implementation of solar-powered drip systems using the low-pressure PC emitters.

5.1.1. Field area

The sensitivity of the cost-optimal design to field area provides insights on both component selection and irrigation scheduling. The physics-based relationship between field area and power system capacity suggests an alternative for irrigation scheduling that would reduce system cost. If larger fields were operated in subsections, the required operating power at any given time would be smaller, which would reduce the power system capacity and cost. As such, operating the system on a sequential irrigation schedule that divides the field into subsections could result in lower cost designs. The optimal designs for this study were all direct-drive designs because batteries and water storage tanks have high replacement and initial costs, respectively. However, if large fields are irrigated in subsections, energy storage options may become cost-effective. In this scenario, the trade-off between decreasing the panel capacity by reducing the system operating point and increasing energy storage capacity would dictate the behavior of the LCC per hectare curve for larger field areas.

For the field area sensitivity analysis, it is also assumed that pump cost scales with maximum pump operating power. This is a reasonable assumption based on the cost of raw materials, but in reality, the pump retail cost is highly dependent on the manufacturer, distributor, and local market conditions. As such, this simplified pump cost model may be under- or overestimating the pump cost, especially for larger fields.

5.1.2. Reliability constraint

The sensitivity study of the cost-optimal design to the reliability constraint, LLPT, shows that a small relaxation of the reliability constraint leads to a large reduction in the optimal system LCC for the baseline case. The point of greatest return on the LLPT sensitivity plot (Fig. 9(a)) is determined by the case definition parameters, namely the selected crop, local weather patterns, soil properties, and the field area. As such, the expected shape of the LLPT sensitivity plot could be predicted for different cases. If the selected crop is highly sensitive to water stress, unlike the olive trees studied here, it can be expected that the LLPT at the point of greatest return will be smaller than 0.1. For fields larger than 2 ha, it can be expected that there is an even greater opportunity for LCC reduction as LLPT increases. Similarly, for locations with high, consistent solar irradiance, such as Morocco, it can be expected that the magnitude of the cost reduction will be similar to that of the case study presented here.

The results also show that a stricter reliability constraint (decreasing LLPT from 0.1 to 0), altered the system design architecture from a

direct-drive design to a design that includes a battery. This indicates that increasing the reliability constraint can eventually force the optimal design to include energy storage options. The numerical threshold of this architectural shift will depend on the specific case, but it will depend on the same parameters that govern the cost trade-off between decreasing system reliability and meeting the crop water demand. The implication is that the case definition and the system operation, i.e. the irrigation amount, can have a significant impact on the optimal design architecture and cost.

5.1.3. Weather variation

Although it was shown that the optimal design for the baseline case is robust to weather variation for the baseline location and crop type, this robustness may not hold for cases with more water-stress sensitive crops or more variable weather conditions. The weather sensitivity analysis presented here can be used to approximate the safety factors on the power system component capacities when designing for such cases. This analysis could also be applied to predict how variation due to climate change might impact system reliability and performance in a given location.

5.2. SDrOP model benchmarking

SDrOP produced an optimal design for the benchmarking case – a 0.52 ha olive orchard in Marrakech, Morocco – that has a power system capacity 7 times smaller and 56% less expensive than that of the commercial software, Compass (Section 4.1). This dramatic size reduction demonstrates the benefits of capturing the behavior and interactions of the subsystems in a single model. Unlike Compass, SDrOP is able to leverage the trade-off between system reliability and component capacities when optimizing for the lowest-cost design. As a result, SDrOP can produce more appropriately-sized pumps and power systems for a given case compared to software tools that do not design systems holistically.

The measured power consumption of a small-scale, low-pressure, PC drip system was compared to the predicted power production of the optimal design for the same field area (Section 4.2.2). Based on the simulated power output, the optimal design would have been able to power 92% of the irrigation events during the field trial. This result provided confidence that SDrOP was able to produce an optimal design, without a priori knowledge of the weather, that would be able to operate reliably in real-world conditions. While further field trial validation is necessary, this result highlights the potential of SDrOP to be used as a design tool for low-cost, solar-powered drip systems on small farms.

5.3. SDrOP model limitations

The field area sensitivity analysis shows that the hydraulic components make up 54–77% of the system LCC, and the initial cost makes up 50–70% of the system LCC. Future work to improve smallholder adoption of drip irrigation should focus on reducing hydraulic costs through layout optimization. Similarly, as smallholders are particularly sensitive to initial cost, government or NGO subsidies could make these systems more accessible to smallholders.

The LLPT sensitivity analysis demonstrated that operational reliability influences the optimal design LCC and component capacities. This suggests that concurrently optimizing the component capacities and the system operation scheme could create further opportunities for system cost reduction. This can be accomplished by converting currently fixed SDrOP parameters – the pump operating point, the timing of panel and energy storage use, and the daily start time of irrigation – into design variables. In addition to further cost reduction, the results of this reformulated optimization problem could provide insight on how to operate the system efficiently and reduce component degradation.

For the Moroccan case studies presented in this paper, the emitters are assumed to be pressure compensating, the layout of the hydraulic network is prescribed, and the pump database is limited to surface, centrifugal pumps. These assumptions are pertinent to the presented cases, but if SDrOP is to be more broadly applicable, its component selection capabilities need to be expanded. The hydraulics module can be adapted to include other irrigation devices, including non-pressure compensating emitters and sprinklers. For cases with groundwater wells, submersible pumps can be included in the database. Further research can be done on the efficiency and cost of the electronic components that interface with the power system and pump. Addressing these limitations could enable further system cost reduction and would make SDrOP more broadly applicable as a tool for designing solar-powered drip irrigation systems.

5.4. Study limitations and future work

Experimental data was used as a benchmark to give confidence that SDrOP was producing realistic optimal designs. This result can be further supported by installing these designs and measuring their reliability in real-world conditions. The next step is to conduct field trials with the optimal designs for various field areas and crops, taking measurements over multiple growing seasons to capture the effects of environmental variability. The results would be used to compare predicted and measured reliability, and to assess the need for a safety factor on the optimal designs.

The sensitivity analyses presented in this paper suggest that further cost reduction can be achieved by irrigating fields in subsections. Future work can determine how to practically operate a field with subsections such that it does not substantially interfere with the users' other tasks. SDrOP can design systems for farms larger than 2 ha, however, to expand the modeling capabilities to larger farms, the operation simulation may need to be modified to reflect how these farmers operate their irrigation on these farms. The practice of deficit irrigation, or water-stressing the crops by irrigating less than the crop water demand, could also be considered as a cost-saving measure. As the LLPT sensitivity analysis shows, a slight decrease in system reliability can lead to significant system cost reduction, so deficit irrigation may be cost-effective without reducing yield for water-stress resistant crops. In addition, a more accurate crop evapotranspiration model could be incorporated in the agronomy module to determine the sensitivity of the optimal design to the crop water demand estimation. The agronomy module presented in this paper is based on FAO 56 and uses a single crop coefficient as a first pass at modeling the agronomy subsystem. This model provides a simple, standardized, conservative estimate of crop water demand known worldwide. However, more detailed agronomy models, such as AquaCrop [39] and dual crop coefficient models, could be employed in future work to analyze the trade-offs between irrigation amount and drip system component capacities as well as provide more robust crop yield estimates.

The actual performance of the optimal design is highly dependent on how the farmer chooses to operate the system. It is ultimately this performance over multiple seasons that will shape the perceived robustness and reliability of these systems and influence adoption among smallholders. As such, any adjustments to irrigation scheduling should be considered in the context of the farmers' needs and expertise. Currently, SDrOP computes the irrigation schedule based on local weather data, crop properties, and local soil properties, but in reality farmers may base their irrigation schedule on the history of a particular field and crop yield. Farmers may have communally-assigned water usage times or amounts, or may be constrained by the cost of water in their location. Therefore, farmers may feel more comfortable using a system that allows them to operate within their unique constraints and preferences. More research should be conducted with farmers to determine their existing agronomic practices and willingness to change those practices with a new technology. In addition, these systems could

be designed to accommodate other tasks, such as storing water for animal husbandry or powering lights, chargers, radios, TVs, etc. Future work will need to analyze a user's willingness to pay for these added features.

6. Conclusions

Smallholder farmers are vital stakeholders in the process of sustainable agricultural intensification, but often lack access to capital, information, and agricultural inputs. This paper presents the Solar-Powered Drip Irrigation Optimal Performance model (SDrOP), a holistic model for optimizing low-cost, solar-powered drip irrigation systems for small farms. The aim of reducing the system cost is to make solar-powered drip irrigation more accessible to smallholders, who are both cost-sensitive and risk-averse. Unlike existing commercial tools, SDrOP captures subsystem interdependencies and leverages the trade-off between system performance and component capacity when optimizing for low-cost designs. The sensitivity analyses conducted in this study provide insights on the system cost-drivers, component selection, irrigation schedule, and robustness to the environment. The sensitivity of LCC to field area revealed market-based and physics-based cost drivers. The former is due to a potential gap in the local pump market for operating low-pressure systems with the novel, low-pressure emitters. The latter is due to the cubic scaling relationship between system operating power and flow rate that is amplified for large field areas. It was also observed that the sensitivity of LCC to the reliability constraint is heavily dependent on case parameters, and that the irrigation schedule influences the cost-optimal design. These results suggest that co-optimizing component capacities and the system operation could enable further cost savings. Finally, it was shown that the optimal design for the baseline case was robust to weather variations, but cases with highly variable irradiance or water-intensive crops may be less robust to environmental variations.

When compared to commercially available software, SDrOP was able to reduce the drip system life cycle cost (LCC) by up to 56% for a benchmark Moroccan olive orchard. In addition, it was shown that a lower-cost optimally designed system could operate an existing small-scale drip system, where 92% of the measured irrigation events fell within the predicted power output range of the optimal system. This comparison provides confidence that SDrOP can produce optimal designs, without a priori knowledge of the local weather, that would operate reliably in real-world conditions. Field trials will be conducted to further validate the SDrOP results, gain insights on system implementation, and to gather feedback from farmers on their perception of the system's value and performance. These factors will ultimately determine the success of the adoption of solar-powered drip irrigation by smallholders.

CRediT authorship contribution statement

Fiona Grant: Conceptualization, Methodology, Software, Formal analysis, Writing – original draft, Visualization. **Carolyn Sheline:** Conceptualization, Methodology, Software, Formal analysis, Writing – original draft, Visualization. **Julia Sokol:** Methodology, Software, Writing – review & editing. **Susan Amrose:** Writing – review & editing, Validation, Funding acquisition. **Elizabeth Brownell:** Investigation, Project administration. **Vinay Nangia:** Resources, Data curation. **Amos G. Winter V:** Supervision, Funding acquisition.

Declaration of competing interest

The authors declare that they have no known competing financial interests or personal relationships that could have appeared to influence the work reported in this paper.

Table 5
Local economic parameters for Morocco.
Source: Cost data sourced from [10] and local contractor invoices.

Parameter	Definition	Unit	Value
$k_{cp,Olive}$	Crop price coefficient	–	0.55
k_i	Installation coefficient	–	0.11
IR	Interest rate	–	0.035 [22]
FR	Inflation rate	–	0.02 [22]
k_m	Maintenance coefficient	–	0.01
UC_{pump}	Pump unit cost	$\left[\frac{\text{USD}}{\text{kW}}\right]$	450
UC_{hyd}	Pipe network unit cost	$\left[\frac{\text{USD}}{\text{ha}}\right]$	2700
UC_{emit}	Emitter unit cost	[USD]	0.05
UC_{pv}	Panel unit cost	$\left[\frac{\text{USD}}{\text{m}^2}\right]$	113
UC_{batt}	Battery unit cost	$\left[\frac{\text{USD}}{\text{kWh}}\right]$	355.32
UC_{tank}	Tank unit cost	$\left[\frac{\text{USD}}{\text{m}^3}\right]$	110

Table 6
PSO algorithm parameters.

Parameter	Value
Swarm size	20
Convergence margin	10 USD
Inertia factor	0.7
Self confidence	1.5
Swarm confidence	1.5
Time step	10
Initial velocity coefficient	30
Convergence steps	10

Funding

This study was supported by USAID Cooperative Agreement Number AID-OAA-A-16-00058, the Julia Burke Foundation, the MIT School of Engineering MathWorks Fellowship, the MIT Lemelson Minority Engineering Presidential Fellowship, and the MIT Mechanical Engineering Department.

Data availability

Data will be made available on request.

Acknowledgments

The authors would like to thank the Institut National de la Recherche Agronomique (INRA) in Morocco for their assistance with the experimental preparations.

Appendix A

A.1. Local cost data

Local cost data were used determine the SDrOP cost parameters. These numbers were obtained while working with the local research partners and contractors. They were converted to unit values when necessary, as seen in Table 5, so they could be applied to a variety of farm sizes.

A.2. PSO algorithm parameters

The following parameters were used in the PSO algorithm. These parameters were selected because they produced repeatable convergence for the range of cases in this study [41,42] (Table 6).

Table 7
AC centrifugal pump models in SDrOP database.

Model name
Lowara 12GS15
Lowara 16GS22
Lowara 1GSL02
Lowara 1GSL03
Lowara 2GS02
Lowara 2GS03
Lowara 32-125-02
Lowara 32-125-03
Lowara 32-160-02
Lowara 32-160-03
Lowara 32-160-05
Lowara 32-200-11
Lowara 32-250-11
Lowara 32-250-15
Lowara 40-200-15
Lowara 40-250-30
Lowara 4GS03
Lowara 4GS05
Lowara 4GS07
Lowara 50-250-30
Lowara 50-250-40
Lowara 6GS05
Lowara 8GS07
Lowara 8GS11
Lowara 8GS15
ecocircB 23-5
ecocircB 6 m
ecocircXLD 40-80-11F
ecocircXL 25-100
ecocircXL 25-40
ecocircXL 32-120F
ecocircXL 32-60
ecocircXL 40-100-12F
ecocircXL 40-180F

A.3. Pump database

The pump database was populated with the following AC centrifugal pump models. These pumps were in the appropriate size range and, based on fieldwork with contractors, their performance characteristics were representative of the locally-available pumps in Morocco (Table 7).

Appendix B. Supplementary data

Supplementary material related to this article can be found online at https://doi.org/10.1016/j.apenergy.2022.119563.

References

[1] International Fund for Agricultural Development (IFAD). Smallholders, food security and the environment. 2013.
[2] Lowder SK, Skoet J, Raney T. The number, size, and distribution of farms, smallholder farms, and family farms worldwide. World Dev 2016;87:16–29.
[3] Rapsomanikis G. The economic lives of smallholder farmers. 2015, Food and Agriculture Organization of the United Nations (FAO).
[4] Larson DF, Otsuka K, Matsumoto T, Kilic T. Should african rural development strategies depend on smallholder farms? An exploration of the inverse productivity hypothesis. 2012, The World Bank.
[5] Rosset P. The multiple functions and benefits of small farm agriculture in the context of global trade negotiations. Development 2000;43(2):77–82.
[6] Burney J, Woltering L, Burke M, Naylor R, Pasternak D. Solar-powered drip irrigation enhances food security in the sudano-sahel. Proc Natl Acad Sci 2010;107(5):1848–53.
[7] Nkya K, Mbowe A, Makoi J. Low-cost irrigation technology, in the context of sustainable land management and adaptation to climate change in the Kilimanjaro region. J Environ Earth Sci 2015;5(7):45–56.
[8] Jägermeyr J, Gerten D, Heinke J, Schaphoff S, Kummu M, Lucht W. Water savings potentials of irrigation systems: global simulation of processes and linkages. Hydrol Earth Syst Sci 2015;19(7):3073–91.
[9] Friedlander L, Tal A, Lazarovitch N. Technical considerations affecting adoption of drip irrigation in sub-Saharan Africa. Agricult Water Manag 2013;126:125–32.
[10] Nangia V, Moussadek R, Montanaro G. Ultra-low energy drip irrigation for MENA countries: Drip irrigation in Morocco. 2017, International Center for Agricultural Research in the Dry Areas (ICARDA).
[11] Agency USEP. EPANet. 1993, https://www.epa.gov/water-research/epanet.
[12] Hutchinson G, Carran P, McIndoe I. IRRICAD: Computerized irrigation design. In: Management of irrigation and drainage systems: integrated perspectives. ASCE; 1993, p. 835–41.
[13] Di Dio P, Provenzano G, Provenzano C, Savona P. IRRIPRO: A Powerful software to graphic and hydraulic design of irrigation plants. In: International conference on agricultural and biosystem engineering for a sustainable world, vol. 1. GRC; 2008, p. 1–14.
[14] Lorentz. Compass. 2010, https://lorentz.com.au/lorentz-compass-pump-design-tool/.
[15] Xylem. Xylect. 2015, https://www.xylect.com/.
[16] Grundfos. Grundfos Product Selection, https://product-selection.grundfos.com/.
[17] Sokol J, Grant F, Sheline C, Winter A. Development of a system model for low-cost, solar-powered drip irrigation systems in the MENA region. In: Volume 2B: 44th design automation conference. American Society of Mechanical Engineers; 2018.
[18] Grant F, Sheline C, Amrose S, Brownell E, Nangia V, Talozi S, Winter A. Validation of an analytical model to lower the cost of solar-powered drip irrigation systems for smallholder farmers in the MENA region. In: Volume 11B: 46th design automation conference. American Society of Mechanical Engineers; 2020.
[19] Kelley LC, Gilbertson E, Sheikh A, Eppinger SD, Dubowsky S. On the feasibility of solar-powered irrigation. Renew Sustain Energy Rev 2010;14(9):2669–82.
[20] Bizimana JC, Richardson JW. Agricultural technology assessment for smallholder farms: An analysis using a farm simulation model (FARMSIM). Comput Electron Agric 2019;156:406–25.
[21] Bakelli Y, Hadj Arab A, Azoui B. Optimal sizing of photovoltaic pumping system with water tank storage using LPSP concept. Sol Energy 2011;85.
[22] Muhsen DH, Khatib T, Abdulabbas TE. Sizing of a standalone photovoltaic water pumping system using hybrid multi-criteria decision making methods. Sol Energy 2017;159:1003–15.
[23] Shamshery P, Winter AG. Shape and form optimization of on-line pressure-compensating drip emitters to achieve lower activation pressure. J Mech Des 2017;140(3).
[24] Sokol J, Amrose S, Nangia V, Talozi S, Brownell E, Montanaro G, Abu Naser K, Bany Mustafa K, Bahri A, Bouazzama B. Energy reduction and uniformity of low-pressure online drip irrigation emitters in field tests. Water 2019;11(6):1195.
[25] Allen RG, Pereira LS, Raes D, Smith M. FAO Irrigation and Drainage Paper No. 56, 1998.
[26] White Box Technologies. Weather data for energy calculations. 2008, http://weather.whiteboxtechnologies.com.
[27] ASHRAE. International weather files for energy calculations 2.0 (IWEC2), https://www.ashrae.org/technical-resources/bookstore/ashrae-international-weather-files-for-energy-calculations-2-0-iwec2.
[28] White F. Fluid mechanics. McGraw Hill; 2011.
[29] Swamee PK, Jain AK. Explicit equations for pipe-flow problems. J Hydraul Div 1976;102(5):657–64.
[30] Jain super flow silver. 2009, Jain Irrigation Systems Ltd.
[31] Jain fertilizer tank gold. 2009, Jain Irrigation Systems Ltd.
[32] Xylem Applied Water Systems. Efficiency Island technical review. 2014, Xylem.
[33] Gülich J. Centrifugal pumps ch. 3.4 dimensionless coefficients, similarity laws and specific speed. 2007, Springer Berlin Heidelberg.
[34] Gülich J. Centrifugal pumps ch. 2 pump types and performance data. 2007, Springer Berlin Heidelberg.
[35] Gülich J. Centrifugal pumps ch. 6.3 determination of the required NPSH. Springer Berlin Heidelberg; 2007.
[36] Villalva MG, Gazoli JR, Filho ER. Comprehensive approach to modeling and simulation of photovoltaic arrays. IEEE Trans Power Electron 2009;24(5):1198–208.
[37] Doorenbos J, Kassam AH. Yield response to water. FAO Irrigation and Drainage Paper No. 33, 1979.
[38] Moriana A, Orgaz F, Pastor M, Fereres E. Yield responses of a mature olive orchard to water deficits. J Am Soc Hortic Sci 2003;128(3):425–31.
[39] Steduto P, Hsiao TC, Fereres E, Raes D. Crop yield response to water. 2012, FAO Irrigation and Drainage Paper No. 66.
[40] Food and Agriculture Organization of the United Nations (FAO). FAOSTAT. 2017, http://www.fao.org/faostat/en/#data/PP.
[41] Grant F. Development and validation of a systems-level cost optimization tool for solar-powered drip irrigation systems for smallholder farms. 2019, Massachusetts Institute of Technology.
[42] Sheline C. Lowering the cost of solar-powered drip irrigation systems for smallholder farmers through systems-level modeling, optimization, and field testing. 2019, Massachusetts Institute of Technology.

[43] Bian DW, Watson SM, Wright NC, Shah SR, Buonassisi T, Ramanujan D, Peters IM. Optimization and design of a low-cost, village-scale, photovoltaic-powered, electrodialysis reversal desalination system for rural India. Desalination 2019;452:265–78.
[44] Hassan R, Cohanim B, de Weck O. A comparison of particle swarm optimization and the genetic algorithm. In: 46th AIAA/ASME/ASCE/AHS/ASC structures, structural dynamics and materials conference. 2005, p. 1897.
[45] Al-Khalidi S. Middle east drought a threat to global food prices. 2014, Reuters.
[46] Demaree-Saddler H. Morocco grain production down 70% on severe drought. 2016, https://www.world-grain.com.
[47] CS6P-270P. 2016, Canadian Solar.